Mon. Not. R. Astron. Soc. **000**, 000–000 (0000) Printed 31 January 2022 (MN LATEX style file v2.2)

How to recover both velocity components in discs of barred galaxies with integral-field spectroscopy

Witold Maciejewski[1⋆], Eric Emsellem[2,3] and Davor Krajnović[2]
[1]*Astrophysics Research Institute, Liverpool John Moores University, Twelve Quays House, Egerton Wharf, Birkenhead, CH41 1LD*
[2]*European Southern Observatory, Karl-Schwarzschild-Str. 2, 85748 Garching, Germany*
[3]*Université Lyon 1, Observatoire de Lyon, Centre de Recherche Astrophysique de Lyon and Ecole Normale Supérieure de Lyon, 9 avenue Charles André, F-69230 Saint-Genis Laval, France*

arXiv:1209.4873v1 [astro-ph.CO] 21 Sep 2012

31 January 2022

ABSTRACT
We present a new method that derives both velocity components in the equatorial plane of a barred stellar disc from the observed line-of-sight velocity, assuming geometry of a thin disc. The method can be applied to large departures from circular motion, and does not require multipole decomposition. It is based on assumptions that the bar is close to steady-state (i.e. does not evolve fast), and that both morphology and kinematics are symmetrical with respect to the major axis of the bar. We derive the equations used in the method, and analyze the effect of observational errors on the inferred velocity fields. We show that this method produces meaningful results via a simple toy model. We also apply the method on integral-field data of NGC 936, for which we recover both velocity components in the disc. Knowing both velocity components in the disc, i.e. the non-observable transverse velocity in addition to the line-of-sight velocity, puts additional constraints on dynamical models and allows for new ways of determining parameters that are crucial in characterizing galaxies.

1 INTRODUCTION

In the last decade, integral-field spectroscopy enabled unprecedented progress in our understanding of the dynamics and evolution of galaxies (e.g. de Zeeuw et al. 2002, Förster Schreiber et al. 2009). With spectra sampled throughout the entire galaxy, regular rotation of the galaxy can be verified and more complex motions can be detected. The nature of these motions is usually recovered by comparing the moments of the line-of-sight velocity distribution (LOSVD) to dynamical models (e.g. Cappellari et al. 2006). However, the signatures expected in the LOSVD may depend on the assumed model, and therefore model-independent signatures, or signatures that depend on minimal number of assumptions, are of great value.

The dependence of the results on the assumed model can be seen on the example of the first moment of the LOSVD, i.e. the line-of-sight velocity, analyzed for non-axisymmetric distortions in a planar flow in a galactic disc. Harmonic analysis was applied to this problem by Franx et al. (1994) and Schoenmakers et al. (1997), but it is limited to small departures from circular motion, and interpreting amplitudes of various multipoles in terms of different physical scenarios is unclear (Wong, Blitz & Bosma 2004). Limiting the expansion to only the initial multipoles distorts the results: when only the $m = 1$ terms are included (radial and tangential velocity), often radial motions of large amplitude are implied (e.g. Swaters et al. 2003). This leads to a continuity problem, as the radially traveling matter should have a source or sink in the galaxy centre. Spekkens & Sellwood (2007) showed that when an $m = 2$ term is added (oval flow), it removes the need for radial bulk motion. Moreover, adding this term changes considerably the derived rotation curve. The difficulty to distinguish radial bulk motion from oval flow has been noticed earlier for radio and long-slit data (e.g. van der Kruit 1974, 1976; Bosma et al. 1977). Thus one needs to characterize non-axisymmetric distortions in the observed kinematics in a way that can be more directly related to the dynamical state of the galaxy.

For a galactic disc, the line-of-sight (LOS) velocity constitutes only one out of the two velocity components. The other component is the transverse velocity in the disc, which generally cannot be determined with the current observing techniques for discs of external galaxies. However, if a galaxy possesses some symmetry, or a steady pattern is present there, one can use these properties to derive the transverse component. This has been done by Sridhar & Sambhus (2003), but it required the knowledge of the angular speed of the rotating pattern, which often cannot be determined with high certainty.

Here we present a new method to derive both velocity components in a disc galaxy that hosts a bar or a dominant bisymmetric perturbation in the stellar component. The two velocity components are recovered from the LOS velocity using the symmetry introduced by the bar, and since the galactic disc needs to be deprojected in this method, the disc inclination and the position angle of its line of nodes must be known. Unlike the previous attempt to model non-circular motions in oval distortions to the gravitational potential (Spekkens & Sellwood 2007), our method is not limited to multiplicity $m \leqslant 2$ — in fact it returns the complete radial and tangential velocity components throughout the disc without the need for multipole expansion.

© 0000 RAS

From the recovered streaming motion one can constrain the bar's contribution to the overall gravitational potential. By applying the continuity equation directly to the two velocity components, one can estimate the pattern speed of the bar.

In Sect.2, we derive the equations through which we recover, from the orientation of the galaxy and the LOS velocity, the radial and tangential velocity components. In Sect.3, we analyze how the recovered values are affected by errors in the adopted orientation of the galaxy. We show how the method presented here works in practice by deriving in Sect.4 the radial and tangential velocity fields in the disc of NGC 936, from the SAURON integral-field data (Krajnović et al. 2011; Emsellem et al. 2012). In Sect.5, we discuss how knowing both components of the velocity field puts better constraints on the structure and dynamics of disc galaxies.

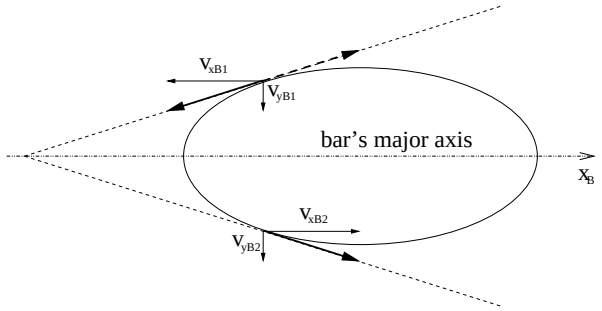


Figure 1. For a star moving in the plane of a barred galactic disc, Cartesian velocity components, in the frame rotating with the bar, are shown at two locations, symmetrical to the bar's major axis (the x_B axis). The thick dashed arrow indicates the velocity vector upon time reversal (see Sect.2).

2 THE METHOD

In this method, we assume that: (1) the bar is in steady-state (it does not evolve fast), (2) the bar is symmetrical with respect to its major axis, (3) the disc of the galaxy is flat, so that there are only two velocity components. The first assumption is well justified by our understanding of evolution of barred galaxies (e.g. Shen & Sellwood 2004). The second one possibly breaks at the ends of the bar, where often a parallelogram-like morphology is seen, particularly when a transition to spiral arms is present. The third assumption may not be valid if the centre of the galaxy is dominated by a bulge. Thus the assumptions of this method are best fulfilled in the middle of the radial extent of the bar. The perturbation caused by the bar is also strongest there.

Imagine a star moving in the disc plane on the trailing side of the bar with velocity v_{B1} in the frame rotating with the bar (Fig.1, where we assume that the bar is rotating counterclockwise). This motion is described by Newtonian dynamics, hence reversing time gives equally possible motion. Upon time reversal, the bar starts rotating clockwise, the star is now on its leading side, and its velocity arrow changes direction (marked by the thick dashed line in Fig.1). If the bar is symmetrical with respect to its major axis, this state upon time reversal is identical to the state on the other side of the bar's major axis before time reversal, i.e. to the star moving with velocity v_{B2}. Thus in a symmetric bar, stars moving on one side of the major axis of the bar with velocities v_{B1} should be mirrored by stars moving on the other side of the bar with velocities v_{B2}. This is true regardless of what orbit the star is on: regular symmetric or not symmetric, or irregular. These orbits are likely to be similarly populated on both sides of the bar, as otherwise the appearance of the bar would not be symmetrical with respect to its major axis. Therefore the *mean* velocity on one side of the bar should be mirrored by that on its other side, and this is the basis of our method. However, in order to emphasize that the star can move from one side of the bar to the other, we connect the two positions in Fig.1 by a simple oval orbit, keeping in mind that our analysis is not limited to such orbits.

Because of the symmetry analyzed above, Cartesian components of the velocity vectors in the frame rotating with the bar, in the plane of the disc, at two locations symmetrical with respect to the bar's major axis are related by

$$v_{xB2} = -v_{xB1} \qquad v_{yB2} = v_{yB1}, \tag{1}$$

where the B index indicates that the x_B axis is aligned with the major axis of the bar. When converted to polar coordinates, the components are related by

$$v_{R2} = -v_{R1} \qquad v_{\varphi 2} = v_{\varphi 1}, \tag{2}$$

with the coordinate system now not dependent on the position of the bar.

If we want to relate the two velocity components in the disc of a galaxy, that is projected on the sky, to the observed LOS velocity, we may impose the Cartesian coordinates in the inertial frame of the disc in such a way that the line-of-nodes (LON) coincides with the x-axis. Then only the y-component of the velocity in the disc will contribute to the observed LOS velocity, and the two are related by[1]

$$v_{LOS} = v'_y \sin i, \tag{3}$$

where the galaxy disc is inclined to the plane of the sky at angle i. The x-component will remain unobservable, constituting exclusively the transverse velocity (i.e. the proper motion), whose vector remains in the plane of the sky.

In the method proposed here, we use the deprojected velocity field v'_y, which can be obtained for the known inclination of the galaxy i and the position angle (PA) of its LON. Then for a disc that contains a steady-state asymmetry, like a bar, we can recover both velocity components using the relation (2) between two independent components at two locations symmetrical with respect to the major axis of the bar. It is possible, because at each of the two locations, the two velocity components contribute differently to v'_y. In Fig.2, the geometry used in deriving formulae for the two velocity components is clarified. The bar is located at an arbitrary angle α to the LON in the plane of the galaxy disc[2]. In the frame rotating with the bar, contributions from the polar velocity components v_R and v_φ to the Cartesian velocity component v_y are

$$v_{y1} = v_{\varphi 1}\cos(\alpha - |\gamma|) + v_{R1}\sin(\alpha - |\gamma|), \tag{4}$$

at position 1, and

$$v_{y2} = v_{\varphi 2}\cos(\alpha + |\gamma|) + v_{R2}\sin(\alpha + |\gamma|), \tag{5}$$

[1] in contrast to velocities measured in the frame rotating with the bar, velocities in the galaxy disc measured in the inertial frame are marked with prime

[2] α is the angle of counterclockwise rotation from the positive half of the LON to the bar's major axis

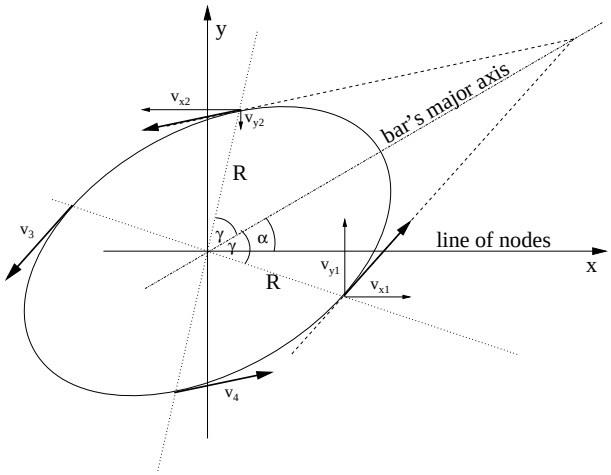


Figure 2. Same as Fig.1, but the LON is now along the Cartesian x-coordinate, and the bar's major axis is at angle α in the galactic plane to the LON. With this choice of coordinates, only the y velocity component contributes to the observed LOS velocity, while the x component is unobservable, remaining in the plane of the sky. This diagram is drawn in the plane of the galactic disc.

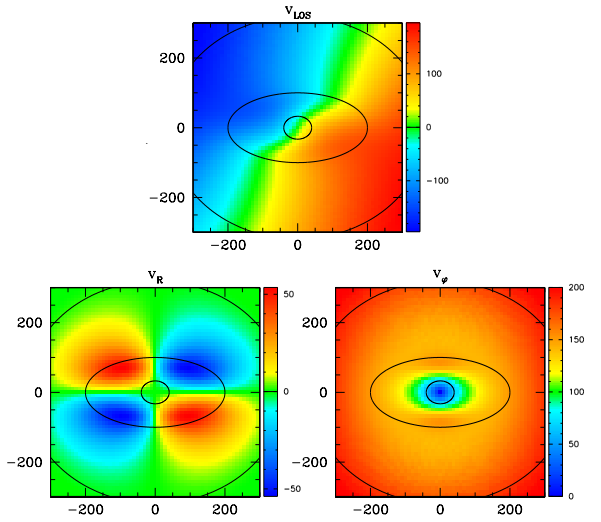


Figure 3. For a cartoon model of an elliptical flow following a bar, defined at the end of in Section 2, we show the deprojected LOS velocity v'_y (*top*), as well as the radial (*bottom-left*) and tangential (*bottom-right*) velocities in the disc plane. Three example oval trajectories are overplotted. The colour scale is shown in the attached wedges. For PA reference, north is up.

at position 2. The angle γ is measured in the plane of the galactic disc, and spans between the bar's major axis and the line connecting each of the two symmetrically located positions, at which v'_y is inferred from the LOS velocity.

The v_y velocity components in (4) and (5) are in the frame rotating with the bar. They can be converted to the inertial frame by adding to v_φ the term $\Omega_B R$, where Ω_B is the angular velocity of the bar, and R is indicated in Fig.2. Thus the y-velocity components in the inertial frame, which directly relate to the LOS velocity through (3), can be written as

$$v'_{y1} = (v_{\varphi 1} + \Omega_B R)\cos(\alpha - |\gamma|) + v_{R1}\sin(\alpha - |\gamma|) \quad (6)$$

$$v'_{y2} = (v_{\varphi 2} + \Omega_B R)\cos(\alpha + |\gamma|) + v_{R2}\sin(\alpha + |\gamma|) \quad (7)$$

As v_{R2} and $v_{\varphi 2}$ are related to v_{R1} and $v_{\varphi 1}$ by (2), substituting (2) to (7) gives

$$v'_{y2} = (v_{\varphi 1} + \Omega_B R)\cos(\alpha + |\gamma|) - v_{R1}\sin(\alpha + |\gamma|). \quad (8)$$

Now there are only two unknowns in the system of two equations (6) and (8): the radial and tangential velocities v_{R1} and $v_{\varphi 1}$, for which the system can be readily solved, yielding

$$v_{R1} = \frac{v'_{y1}\cos(\alpha + |\gamma|) - v'_{y2}\cos(\alpha - |\gamma|)}{\sin(2\alpha)} \quad (9)$$

$$v_{\varphi 1} = \frac{v'_{y1}\sin(\alpha + |\gamma|) + v'_{y2}\sin(\alpha - |\gamma|)}{\sin(2\alpha)} - \Omega_B R \quad (10)$$

Thus if the galaxy is symmetrical with respect to the major axis of its bar, one can recover both velocity components in the disc plane *in the inertial frame*: v_{R1} and $v_{\varphi 1} + \Omega_B R$. Note that for this we use the *deprojected* velocity field v'_y, hence the galaxy has to be deprojected before applying this method. In Sect.4, we show how this procedure works in practice. Because of the singularity in the denominator in (9) and (10), this method fails when $\sin(2\alpha) = 0$, i.e. for the bar either parallel or perpendicular to the LON. One can expect best results for the bar at moderate angles to the LON.

We visualize the expected results by showing in Fig.3 the radial and tangential velocity components for a cartoon model of an elliptical flow. In arbitrary units, this model assumes a rotation curve that rises up to the radius of 200, and is flat further out at the amplitude of 200 arbitrary units. The motion is circular outside the radius of 400, but it becomes elliptical inside that radius, which is intended to mimic the motion in a bar. The elliptical motion reaches maximum eccentricity at semi-major axis $a = 200$, where the axis ratio is $b/a = 0.5$. The motion further inside is becoming increasingly circular, which intends to simulate the area dominated by the bulge. The elliptical flow intended to follow the bar rotates like a solid body with respect to the inertial frame, with corotation radius at 400. Three example oval trajectories, including the most eccentric one, are overplotted in Fig.3.

The top panel of Fig.3 displays the deprojected LOS velocity v'_y, when the PA[3] of the bar is 90°, and that of the LON is 240°. One can notice an asymmetry caused by the elliptical flow. Its most evident signature can be seen in the radial velocity component (bottom-left panel of Fig.3) in the form of four velocity extrema in four quadrants: two maxima and two minima, alternately. The signature is strong: in our cartoon model with the maximum eccentricity of the flow being $b/a = 0.5$, it has an amplitude of 54 for the rotation curve at the amplitude of 200 in its flat part. As expected, the signal is strongest where the flow is most eccentric. The tangential velocity component, shown in the bottom-right panel of Fig.3, displays complex structures that have no straightforward correspondence to the structure of the flow. By experimenting with various additional cartoon models, we noticed that these structures strongly depend on the variation of the eccentricity of the flow and on the adopted rotation curve, while the structure of the radial velocity component, shown in the bottom-left panel of Fig.3, remains virtually unchanged. As expected, using equations (9) and (10) we can recover the radial

[3] PA is measured east of north, to the positive half of the LON in kinematics

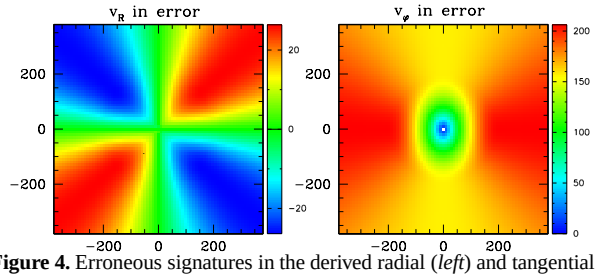


Figure 4. Erroneous signatures in the derived radial (*left*) and tangential (*right*) velocity fields in the disc plane, caused by adopting the PA of the LON being 5° in error, while the actual motion is purely circular with the rotation curve same as in Fig.3. The velocity fields were derived using (9) and (10) with the alleged bar at $\alpha = 20°$ to the adopted LON, and horizontal in these plots. The colour scale is shown in the attached wedges.

and tangential velocity fields in the lower panels of Fig.3 from the deprojected LOS velocity v'_y in the top panel of Fig.3.

3 EFFECTS OF OBSERVATIONAL ERRORS

In addition to the accuracy in measurement of the LOS velocity itself, the structure and the amplitude of the derived two velocity components in the disc plane can be affected by observational errors in the systemic velocity of the galaxy, the inclination of the disc, as well as in the position angles of the bar's major axis and of the LON.

3.1 Error in the PA of the LON

The potentially most problematic source of error is the uncertainty on the PA of the LON, as one signature that it creates is similar to that of the oval flow. In Fig.4, we show erroneous radial and tangential velocity fields that our method produces for a disc in purely circular rotation, when the PA of the LON is 5° in error. We adopted here the same rotation curve as in Sect.2. If the PA of the LON were correct, the tangential velocity field should be axisymmetric, while the radial velocity field should be uniformly zero.

The erroneous signature in the radial velocity field in the left panel of Fig.4 resembles the signature of real oval flow in the bottom-left panel of Fig.3. Both are of bisymmetric nature, with opposite extrema in each quadrant. However, there is one major difference between these signatures: while the signature of a real oval flow is strongest at the radius where the flow is most eccentric (Fig.3, bottom-left panel), signature of the misplaced LON continues to arbitrarily large radii (Fig.4, left panel). Therefore in order to assure that the radial motion recovered with our method is genuine, it is essential that in addition to sampling the region where the flow is expected to be non-circular, the region outside is sampled as well.

The magnitude of the error in the derived radial velocity changes with the PA of the bar relative to the LON (the α angle in our method), being largest when the bar is parallel or perpendicular to the LON. The error in the left panel of Fig.4 is showed for α =20°, for which it reaches the magnitude of 26 (for reference, the flat part of the rotation curve in the same units is at 200). The error has the same pattern and magnitude when the bar is 20° from the direction perpendicular to the LON, i.e. for α =70°. For α =10° or 80°, the magnitude reaches 51, while for α =40° or 50°, it is reduced to 15. Clearly, the radial velocity field is least affected by the error in the PA of the LON when the angle α between the LON and the bar is around 45° or 135°.

When the tangential velocity field is derived with our method for purely circular rotation, but with the PA of the LON in error, it is no longer axially symmetric, but it develops another bisymmetric pattern, now with two maxima and two minima along the bar's major axis and perpendicular to it (Fig.4, right panel). Like in the case of the derived radial velocity, the magnitude of the error in the derived tangential velocity changes with α, and is minimized for α around 45° or 135°. In Fig.4, the derived tangential velocity field is shown for α =20°. In the flat part of the rotation curve, where it should be constant, it varies between 156 and 206. Thus the amplitude of variation is 25, similar to that in the radial motion, and the average tangential velocity is 181, smaller than the rotation curve in the flat part, which is 200. When α =10°, the amplitude of variation in the derived tangential velocity increases to 47, and its average is at 157. The same variation is for α =80°, but then the average is 240. Thus a bisymmetric pattern in the derived tangential velocity field similar to that in the right panel of Fig.4 can serve as indicator of an incorrect PA of the LON adopted for this derivation. As can be seen in Fig.3, it should not accompany a genuine streaming observed in radial motion.

3.2 Inclination and bar PA errors

The error in the disc inclination propagates from (3) to (9) and (10) as a multiplicative constant, hence it affects the amplitude of both radial and tangential motion, as expected. Incorrect deprojection of the disc can also result in spurious signatures in radial and tangential velocity field similar to those in Fig.4, even if the disc is in purely circular motion and the LON is identified correctly. However, the amplitudes of these signatures are considerably smaller than those of the signatures indicating an error in the position angle of the LON that we described in Sect.3.1. The error in inclination must be at least 30° in order to generate the amplitude of signatures the same as in the case of the PA of the LON being 5° in error.

In order to estimate the error in the derived velocity field caused by adopting an incorrect PA of the bar, we derived the radial and tangential velocity fields for the oval motion described in Sect.2, but for the PA of the bar in the disc plane being 5° in error. The structure of the derived radial velocity field, shown in the bottom-left panel of Fig.3, remains virtually unaffected by this error: its bisymmetric structure remains the same, and its amplitude is altered only by 5%. The structure also gets stretched along the bar, but its aspect ratio does not change by more than 10%. Most importantly, contrary to the error in the PA of the LON, which produces signatures in the radial velocity field that extend to arbitrarily large radii (Fig.4, left panel), such signatures are absent when the PA of the bar is in error.

The structure of the tangential velocity field changes moderately because of the PA of the bar being in error: the rate of growth along the bar, and the magnitude of the local maximum on bar's minor axis change by a factor less than 10%. Like the radial velocity field, the tangential velocity field is affected by an error in the bar's PA only within the bar. At larger radii it is axisymmetric, even when the PA of the bar is in error. No bisymmetric structure like that from the right panel of Fig.4 is

seen, which indicates that such a structure is a unique signature of an incorrect PA of the LON.

3.3 Error in the systemic velocity of the galaxy

The error ϵ in the systemic velocity, when $v'_{y1}+\epsilon$ and $v'_{y2}+\epsilon$ are being used in (9) and (10) instead of v'_{y1} and v'_{y2}, propagates to the derived radial and tangential velocity components in such a way that the erroneous values, v^{ϵ}_{R1} and $v^{\epsilon}_{\varphi 1}$, relate to the correct ones by

$$v^{\epsilon}_{R1} = v_{R1} - \epsilon\frac{\sin|\gamma|}{\cos\alpha} \quad (11)$$

$$v^{\epsilon}_{\varphi 1} = v_{\varphi 1} + \epsilon\frac{\cos|\gamma|}{\cos\alpha}. \quad (12)$$

As $v_{R2} = -v_{R1}$, this generates an $m = 1$ mode in the radial velocity field. However, this effect can be completely removed by invoking the symmetry with respect to the *minor* axis of the bar. In Fig.2, we used two LOS velocities, v'_{y1} and v'_{y2}, at two locations, $\alpha \pm \gamma$, symmetric with respect to the major axis of the bar, in order to obtain the two velocity components in the disc, v_{R1} and $v_{\varphi 1}$. Similarly, at locations $\alpha + \pi \pm \gamma$, i.e. on the other side of the minor axis of the bar, one can derive the two velocity components, v_{R3} and $v_{\varphi 3}$ from the LOS velocities v'_{y3} and v'_{y4}. If the flow is symmetric with respect to the minor axis of the bar then these components should be equal to v_{R1} and $v_{\varphi 1}$. The v_{R3} and $v_{\varphi 3}$ velocity components can be derived from equations analogous to (9) and (10):

$$v_{R3} = \frac{v'_{y3}\cos(\alpha+\pi+|\gamma|) - v'_{y4}\cos(\alpha+\pi-|\gamma|)}{\sin(2(\alpha+\pi))} \quad (13)$$

$$v_{\varphi 3} = \frac{v'_{y4}\sin(\alpha+\pi+|\gamma|) + v'_{y4}\sin(\alpha+\pi-|\gamma|)}{\sin(2(\alpha+\pi))} - \Omega_B R. \quad (14)$$

If v'_{y3} and v'_{y4} are affected by the same error in the systemic velocity ϵ as v'_{y1} and v'_{y2} are affected above, the error propagates to v_{R3} and $v_{\varphi 3}$ yielding erroneous values v^{ϵ}_{R3} and $v^{\epsilon}_{\varphi 3}$ that relate to the correct ones by

$$v^{\epsilon}_{R3} = v_{R3} - \epsilon\frac{\sin|\gamma|}{\cos(\alpha+\pi)} = v_{R3} + \epsilon\frac{\sin|\gamma|}{\cos\alpha} \quad (15)$$

$$v^{\epsilon}_{\varphi 3} = v_{\varphi 3} + \epsilon\frac{\cos|\gamma|}{\cos(\alpha+\pi)} = v_{\varphi 3} - \epsilon\frac{\cos|\gamma|}{\cos\alpha}. \quad (16)$$

By comparing (15) and (16) to (11) and (12) one can see that the error in v_{R3} and $v_{\varphi 3}$ is of the same magnitude, but of opposite sign compared to that in v_{R1} and $v_{\varphi 1}$. Since from symmetry $v_{R3} = v_{R1}$ then averaging v^{ϵ}_{R1} and v^{ϵ}_{R3} cancels the error originating from the incorrect systemic velocity. The same is true for $v_{\varphi 3}$ and $v_{\varphi 1}$. In both cases, the symmetrization can be written as

$$v^{\rm symmetrized}(x,y) = \frac{v(x,y) + v(-x,-y)}{2}. \quad (17)$$

Certainly the price for this averaging is the loss of information about possible difference in velocity structure on the two sides of the minor axis of the bar. However, if this difference is not caused by inaccurate derivation, but is rather intrinsic to the galaxy itself, then it is likely that the velocities are not symmetrical with respect to the *major* axis of the bar, either. Thus the method presented here is rather unlikely to recover differences in kinematical structure at the two ends of the bar. Note that the symmetrization is the last, additional step of our method, after the radial and tangential velocities have been determined independently on the two sides of the minor axis of the bar, and therefore it does not affect the method. It can be performed optionally, if one wants to remove the effects of error in systemic velocity.

Table 1. Parameters of NGC 936

	K83	KG89	A3D	adopted
recession velocity [km s^{-1}]	–	–	1429	1429
PA of photometric major axis	136°	135°	130.7°	–
PA of kinematic major axis	–	–	318.0°	318°
inclination (0° for face-on)	40.9°	41°	39°	39°
PA of the bar on the sky	77°	79°	–	81°
α between LON and bar	114.4°	–	–	117°

Abbreviations for the sources of parameter values are: K83 – Kormendy (1983, note: inclination converted from a convention 0° for *edge-on* there), KG89 – Kent & Glaudell (1989), A3D – Cappellari et al. (2011), Krajnović et al. (2011)

3.4 Summary of effects of observational errors

In summary, the error in the PA of the LON is the strongest source of uncertainty in the derived velocity fields. However, this error can be easily spotted, as it generates a unique signature of bisymmetry in the derived tangential velocity (Fig.4, right panel), and its signature in the derived radial velocity field (Fig.4, left panel) is different at large radii from the signature of genuine streaming motion (Fig.3, bottom-left panel). Errors in the inclination and in the PA of the bar affect the derived velocity field in lesser degree, while the error in the systemic velocity has no effect if the velocity field is symmetrized with respect to the minor axis of the bar.

4 APPLICATION TO THE SAURON IFU DATA OF NGC 936

NGC 936 is a barred S0 galaxy, whose morphology and kinematics have been studied in detail in the pre-IFU era (Kormendy 1983, 1984; Kent 1987; Kent & Glaudell 1989, Merrifield & Kuijken 1995). It is very luminous and hence massive, which helps maximizing the measured LOS velocities. Because of the strong bar present in NGC 936, the amplitude of non-circular motions is expected to be large as well. The bar in NGC 936 is not nearly aligned with either principal axis, which minimizes errors caused by adopting inaccurate geometry, as analyzed in Sect.3.

Here, we apply the method described in Sect.2 in order to recover the radial and tangential velocities from the integral-field data of NGC 936 observed with the SAURON integral-field spectrograph (Bacon et al. 2001) mounted on the William Herschel telescope in La Palma. In total, 40 exposures were obtained, covering the full extent of the bar, during a run of 5 consecutive nights in August 2003, with a few additional exposures in January 2004. The data were reduced as in Emsellem et al. (2004), and all exposures merged into a single mosaic datacube. These data have been obtained in the course of a programme to observe barred galaxies with SAURON (PI. Emsellem), and the resulting mosaic has been used in the course of the ATLAS$^{\rm 3D}$

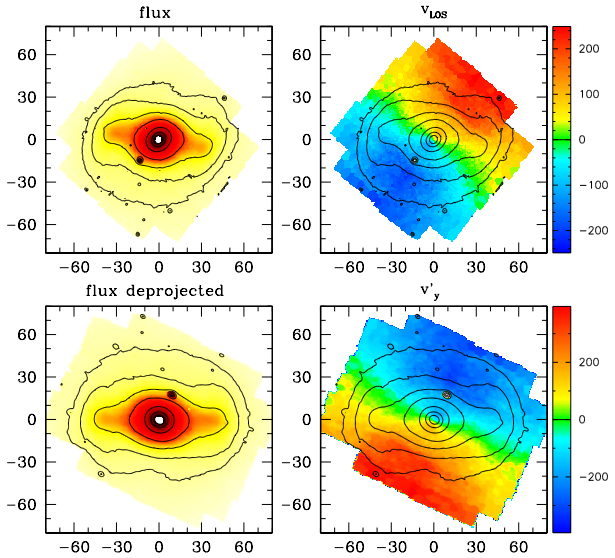


Figure 5. *Top-left:* The image of NGC 936 taken from the zeroth moment of the full mosaic SAURON datacube. *Top-right:* The LOS velocity (the first moment) of NGC 936 from the full mosaic SAURON datacube, after subtraction of the systemic velocity. North is up in the upper panels. *Bottom-left:* The image of NGC 936, deprojected using parameters from Table 1, and rotated so that the bar is horizontal. *Bottom-right:* The LOS velocity, deprojected and rotated in the same way as the image, and scaled by $\sin i$, so that it results in the v'_y velocity component in the disc plane of NGC 936, perpendicular to the LON. The bright point-like source is the Supernova 2003gs. Isophotes are overplotted in contour. The colour scale is shown in the attached wedges. The linear scale is in arcsec in the upper panels, and in arcsec deprojected to the disc plane in the lower panels.

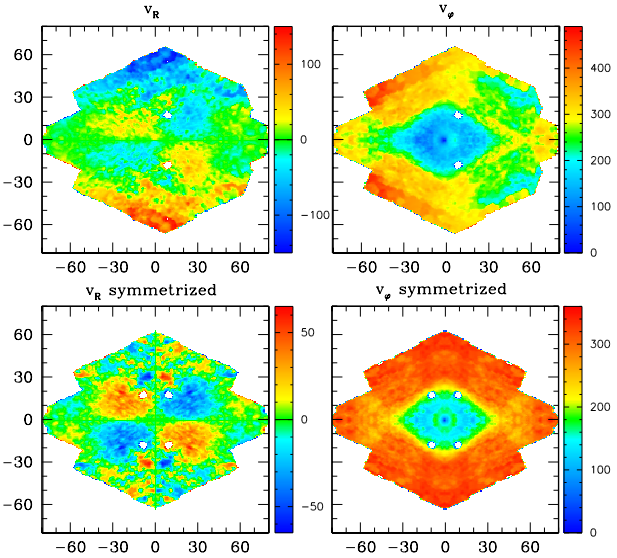


Figure 6. *Top-left:* The radial velocity field in the disc of NGC 936, derived from (9). *Top-right:* The tangential velocity field derived from (10). *Bottom-left:* The radial velocity field symmetrized around the minor axis of the bar (after averaging velocities on the left and right of the minor axis of the bar). *Bottom-right:* The tangential velocity field, symmetrized in the same way. The point-like sources are mirror images of the supernova. The bar is horizontal. The colour scale is shown in the attached wedges. The linear scale is in arcsec deprojected to the disc plane.

project (Cappellari et al. 2011) as NGC936 is part of that sample. The maps presented here (see Krajnović et al. 2011) will also be part of a paper presenting the mosaic in greater detail (Emsellem et al. 2012). Note that the bright point-like source present on the South-Eastern side of the centre of the galaxy is a Supernova (2003gs) discovered by Robert Evans which was still visible during the first run in August 2003. Parameters of NGC 936 derived in previous studies and adopted here are listed in Table 1. Below we list the steps in which the observed two-dimensional LOS velocity array was processed in order to derive the two velocity components in the disc of the galaxy.

Firstly, the systemic velocity was subtracted from the observed LOS velocity. The systemic velocity was derived from the heliocentric recession velocity of 1429 km s^{-1}listed in the ATLAS^{3D} survey (Cappellari et al. 2011), after subtracting the heliocentric correction of 24 km s^{-1}. Thus the systemic velocity in the data is 1405 km s^{-1}.

Secondly, in order to obtain v'_y in the galaxy plane from (3), the LOS velocity field was deprojected, assuming the PA of the LON at 138° (318° for its positive half) and the disc inclination of 39°. All the sources listed in Table 1 are in good agreement about the inclination value. On the other hand, the ATLAS^{3D} estimate of the PA of the photometric major axis (Krajnović et al. 2011) gives a value 4°-5° smaller than earlier estimates (Kormendy 1983; Kent & Glaudell 1989), while ATLAS^{3D} estimate of the PA of the kinematic major axis is 2°-3° larger than those estimates. We adopt here the kinematic estimate, acknowledging that it may be in error by up to 5°. We explored consequences of this uncertainty with similar magnitude in Sect.3.1.

Thirdly, the derived v'_y velocities at locations symmetrical with respect to the bar's major axis were substituted to (9) and (10) in order to recover v_R and v_φ. In order to use this symmetry, we tried to rotate the bar to the horizontal position using the PA of the bar given by Kormendy (1983) and Kent & Glaudell (1989), but this was resulting in a slightly non-horizontal bar. We had to modify the PA of the bar to 81° in order to alleviate it, and this is the PA that we consequently use. Our adopted angle between the positive half of the LON and the bar on the sky is therefore $\alpha_{\rm sky} = 123°$. After deprojection, the angle between the LON and the bar *in the plane of the galaxy disc* is $\alpha = 117°$, as $\tan\alpha = \tan\alpha_{\rm sky}/\cos i$.

The integrated luminosity derived from the full mosaic datacube is shown in the top-left panel of Fig.5. In the top-right panel, we show the LOS velocity field (the first moment of the SAURON data), after correction for the systemic velocity. The deprojected image of NGC 936, rotated so that the bar is horizontal, is shown in the bottom-left panel of Fig.5. The same deprojection and rotation was applied to the LOS velocity field. In addition, the deprojected LOS velocity was divided by $\sin i$ in order to obtain the velocity component perpendicular to the LON in the disc plane of NGC 936 (v'_y velocity in our method). This v'_y velocity field, shown in the bottom-right panel of Fig.5, is used as the input in the method presented here.

The derived radial and tangential velocity fields are shown in the upper panels of Fig.6. The fields are smaller than the deprojected velocity field from the bottom-right panel of Fig.5, because they could be created only when information from both sides of the bar is available. In the region dominated by the bar, the pattern in the derived radial velocity of NGC 936 resembles the cartoon model from the bottom-left panel of Fig.3:

it is bisymmetric ($m = 2$), with maxima and minima in the quadrants defined by the bar. The appearance of the extrema is somewhat different on the two sides of the minor axis of the bar, with their shapes stretched along the bar on the left, and more confined on the right. This may hint at somewhat different kinematics at the two ends of the bar in NGC 936. Outside the bar, there is a clear $m = 1$ pattern with a strong minimum at the top and a maximum at the bottom. In Sect.3.3, we showed that an $m = 1$ pattern can be caused by an error in the systemic velocity. Kinemetry fit (Krajnović et al. 2006) to the LOS velocity field of NGC 936 shows that the mean velocity rises almost monotonically in the inner 60 arcsec by 25 km s^{-1}. Therefore adopting for the systemic velocity the mean velocity in the inner parts of the galaxy, as we did here, results in a velocity asymmetry for the outer parts. Our method generates a typical signature of $m = 1$ multiplicity in the outer parts, seen in the top-left panel of Fig.6. Averaging over the two ends of the bar naturally removes this effect, and it is performed below. The tangential velocity field (Fig.6, top-right) well recovers the rise of the rotation curve to about 250 km s^{-1} in the inner 30 arcsec, but it is highly asymmetric at larger radii. Upon closer inspection, antisymmetry with respect to the minor axis of the bar dominates there, hence averaging over the two ends of the bar should return a more reliable velocity field, and it is performed below.

The symmetrized radial and tangential velocity fields, after symmetrization using (17), are shown in the lower panels of Fig.6. The symmetrization of the radial velocity field removes strong extrema of $m = 1$ multiplicity that were present at the top and bottom of this field, and now the bisymmetric pattern dominates the field, having largest amplitude within the bar. The pattern does not continue to larger radii, hence it is a genuine signature of streaming motion, and not of an error in the PA of the LON. The amplitude of radial velocity reaches 60 km s^{-1} locally, but after averaging over small fluctuations, it is in the range 30-40 km s^{-1}. When compared to the amplitude of the flat part of the rotation curve of about 300 km s^{-1} (see below), this relative amplitude is 2-3 times smaller than in the cartoon model from Sect.2. Outside the bar, there is a hint of another, weaker bisymmetric pattern of opposite sign at large radii. It may be related to change in the direction of major axis of orbits outside the corotation of the bar, in the outer disc, or it may indicate that the PA of the LON or the inclination is in slight error. In any case, this signature is much weaker (below 10 km s^{-1}) than the dominating signature of streaming motion in the bar.

The azimuthal dependence of the derived tangential velocity, seen in the top-right panel of Fig.6, has been largely removed after the field has been symmetrized around the minor axis of the bar (Fig.6, bottom-right panel). Now the symmetrized tangential velocity field agrees well with the cartoon model: it not only recovers the rise of the rotation curve in the inner 30 arcsec, but also its flat part at larger radii, where it reaches amplitude of about 300 km s^{-1}. However, the symmetrized tangential velocity still shows some azimuthal variation at large radii between 320 km s^{-1} near the minor axis of the bar and 280 km s^{-1} near the major axis, with one feature as low as 260 km s^{-1}. This is consistent with the PA of the LON or the inclination being in slight error, but that does not dominate the recovered signal.

5 DISCUSSION

Transverse velocity can be observed as proper motion only for stars in our Galaxy and nearby objects. This motion is too small to be observed in external galaxies besides our nearest neighbours. However, if some degree of symmetry is assumed in the system, this unobservable velocity component can be deduced from the LOS velocity and the galaxy orientation in space. The method presented here involves the symmetry of the flow with respect to the major axis of the bar. It assumes geometry of flat disc, hence it neglects the vertical dimension in the disc. Inclusion of a vertical spatial extent, like in a thick disc or a bulge, will introduce projection effects, important for highly inclined discs. Inclusion of a vertical velocity component will not change the results presented here as long as there is no vertical bulk motion, so that random motions contributing to the vertical velocity dispersion dominate. Vertical bulk motion can affect the radial and tangential velocity components derived with the method presented here, but it can exist only when the disc warps from a plane. Warps within bars have not been observed, but similar effect can be caused by a buckling bar, which has been theoretically predicted (Binney 1981; Combes & Sanders 1981). In Sect.2, we noted that this method assumes a steady-state bar, which excludes a quickly evolving buckling bar. In a separate paper devoted to the analysis of the integral-field spectra of NGC 936 (Emsellem et al. 2012), we will build N-body models of this galaxy, and will search for significant vertical bulk motions.

The method presented here can be applicable to stars, because of time reversibility in dissipationless Newtonian dynamics, but not to gas, which is dissipational. Gas flows on the two sides of the major axis of the bar differ considerably (e.g. Athanassoula 1992), and with our method one cannot retrieve two velocity components of gas flow in a bar, and thus explicitly derive the inflow rate. Below we present implications of knowing the two-dimensional *stellar* velocity field.

5.1 Possible advantages of knowing both velocity components

Knowing both velocity components in the disc clearly provides better constraints on dynamical models. The method presented here recovers these components in a non-parametric way, without multipole expansion. It has been shown (Spekkens & Selwood 2007) that limiting the number of terms in the multipole expansion can greatly alter the rotation curve, in addition to predictions of significant radial flow that causes the 'continuity problem'.

The only explicit way to derive angular velocity of a rotating pattern, the Tremaine-Weinberg method (Tremaine & Weinberg 1984), relies on the continuity equation applied to the fluid of stars moving in a flat disc of a galaxy, in which a pattern rotating with a well defined angular velocity is present. The continuity equation in the plane of the disc involves, at any location, surface density of the tracer, as well as both its velocity components. As only one velocity component can be observed, Tremaine and Weinberg performed apt integrations, so that the dependence on the unobserved velocity component can be removed, and in effect, the angular velocity of the pattern derived. Because of the need for such integration, the Tremaine-Weinberg method involves integrals extending to infinity, but it has been shown that it gives reliable estimates when integrals

include the majority of the galactic emission (e.g. Aguerri, Debattista & Corsini 2003).

Once we recover *both* velocity components in a disc of a barred galaxy with our method, the continuity equation can be solved for pattern speed at any location independently, without the need of integrating this equation. This should allow studies of spatial dependence of pattern speed similar to those of radial dependence (Merrifield, Rand & Meidt, 2006; Meidt et al. 2008). However, as can be seen in Fig.6, the derived velocity field is noisy, and it must be spatially averaged before any conclusions on pattern speed can be made. We are currently searching for the most efficient scheme of averaging.

Gravitational potential of the bar exerts torques that induce non-circular motion of stars. Previously, bar torque was estimated e.g. from near-IR photometry (Laurikainen & Salo 2002; Speltincx, Laurikainen & Salo 2008) or by comparing the simulated velocity fields of the gas component to the observed H_α, CO or HI velocity fields (Kranz, Slyz & Rix 2003; Boone et al. 2007). This requires a large suite of hydrodynamical models and/or estimates on mass-to-light ratio. In our method, constraints on the bar contribution to the total gravitational potential can be derived from the amplitude of the streaming motion in the bar, in particular the amplitude of the radial motion. This amplitude, normalized to the rotation curve, is proportional to the bar torque, normalized by the total radial force. The radial force characterizes the total gravitational potential, while torque is likely to come exclusively from the bar. Thus in this way we can estimate the bar contribution that is independent of the mass-to-light ratio, which is the source of bias in the photometric estimates.

6 CONCLUSIONS

We have presented a new method to derive both velocity components in a barred stellar disc from the observed LOS velocity. The method relies on symmetry of the flow around the major axis of the bar, but it is readily generalized for flows having other azimuthal periodicities (like lop-sided distributions). The method does not use multipole expansion and is not limited to small departures from circular motion. It provides best results when the bar is not close to being parallel or perpendicular to the LON, and the integral-field data cover the whole bar, extending somewhat beyond it. The values of the two derived velocity components are most affected by an error in the PA of the LON, but if the derived values are in error, a clear signature appears in the derived velocity field. We applied the method to the SAURON integral-field data of NGC 936 (Krajnović et al. 2011; Emsellem et al. 2012) and recovered patterns in the radial and tangential velocity field, which we expected based on a cartoon model of a simple generic oval flow. The method can be readily applied to barred galaxies observed in recent surveys, which cover the whole extent of the galaxy disc, like the VENGA (Blanc et al. 2010) and CALIFA (Sanchez et al. 2012) surveys. Future wide-field integral-field units, like MUSE (Laurent et al. 2010), will provide data ideally suited for this method. Having both velocity components in the disc puts better constraints on dynamical models, and opens new ways to determine the mass and the pattern speed of the bar.

An Interactive Data Language implementation of the method presented in this paper is available at the web address: http://www.eso.org/∼dkrajnov/idl. WM wishes to thank the European Southern Observatory for supporting this work during his research stay as a Visiting Fellow in November-December 2011 at ESO Headquarters in Garching/Germany.

REFERENCES

Aguerri, J., Debattista, V. P. & Corsini, E. M. 2003, MNRAS, 338, 465
Athanassoula, E. 1992, MNRAS, 259, 345
Bacon, R. et al. 2001, MNRAS, 326, 23
Binney, J. 1981, MNRAS, 196, 455
Blanc, G. A. et al. 2010, ASP Conerence Series, Vol. 432, p.180
Boone, F. et al. 2007, A&A, 471, 113
Bosma, A., van der Hulst, J. M., & Sullivan, W. T. 1977, A&A, 57, 373
Cappellari, M. et al. 2006, MNRAS, 366, 1126
Cappellari, M. et al. 2011, MNRAS, 413, 813
Combes, F. & Sanders, R. H. 1981, A&A, 96, 164
de Zeeuw, P. T. et al. 2002, MNRAS, 329, 513
Emsellem, E. et al. 2004, MNRAS, 352, 721
Emsellem, E. et al. 2012, in preparation
Förster Schreiber, N. et al. 2009, ApJ, 706, 1364
Franx, M., van Gorkom, J.H. & de Zeeuw, T. 1994, ApJ, 436, 642
Kent, S. M. 1987, AJ, 93, 1062
Kent, S. M. & Glaudell, G. 1989, AJ, 98, 1588
Kormendy, J. 1983, ApJ, 275, 529
Kormendy, J. 1984, ApJ, 286, 132
Krajnovic, D. et al. 2006, MNRAS, 366, 787
Krajnovic, D. et al. 2011, MNRAS, 414, 2923
Kranz, T., Slyz, A., & Rix, H.-W. 2003, ApJ, 586, 143
Laurent, F. et al. 2010, SPIE Conference Series, 7739, 147
Laurikainen, E. & Salo, H. 2002, MNRAS, 337, 1118
Meidt, S.E. et al. 2008, ApJ, 676, 899
Merrifield, M. R. & Kuijken, K. 1995, MNRAS, 274, 933
Merrifield, M. R., Rand, R.J. & Meidt, S.E. 2006, MNRAS, 366, L17
Sanchez, S.F. et al. 2012, A&A, 538, A8
Schoenmakers, R.H.M., Franx, M. & de Zeeuw, P.T. 1997, MNRAS, 292, 349
Shen, J. & Sellwood, J. A. 2004, ApJ, 604, 614
Spekkens, K. & Sellwood, J. A. 2007, ApJ, 664, 204
Speltincx, T., Laurikainen, E. & Salo, H. 2008, MNRAS, 383, 317
Swaters, R.A. et al. 2003, ApJ, 587, L19
Sridhar, S. & Sambhus, N. 2003, MNRAS, 345, 539
Tremaine, S. & Weinberg, M. D. 1984, ApJ, 282, L5
van der Kruit, P. C. 1974, ApJ, 188, 3
van der Kruit, P. C. 1976, A&A, 52, 85
Wong, T., Blitz, L., & Bosma, A. 2004, ApJ, 605, 183